Research article

JGS
Journal of the Geological Society

https://doi.org/10.1144/jgs2023-155 | Vol. 181 | 2024 | jgs2023-155

Marine redox dynamics and biotic response to the mid-Silurian Ireviken Extinction Event in a mid-shelf setting

Yuxuan Wang[1*], Paul B. Wignall[1], Yijun Xiong[1], David K. Loydell[2], Jeffrey Peakall[1], Jaco H. Baas[3], Benjamin J. W. Mills[1] and Simon W. Poulton[1]

[1] School of Earth and Environment, University of Leeds, Leeds LS2 9JT, UK
[2] School of the Environment, Geography and Geosciences, University of Portsmouth, Burnaby Road, Portsmouth PO1 3QL, UK
[3] School of Ocean Sciences, Bangor University, Menai Bridge LL59 5AB, UK
YW, 0000-0001-9266-1778
*Correspondence: eeywan@leeds.ac.uk

Abstract: The early Silurian Llandovery–Wenlock boundary interval is marked by significant marine perturbations and biotic turnover, culminating in the Ireviken Extinction Event and the Early Sheinwoodian Carbon Isotope Excursion. Here, we apply multiple independent redox proxies to the early Wenlock Buttington section, which was deposited in a mid-shelf location in the Welsh Basin, UK. To account for the regional geochemical variability in marine sediments due to factors such as sediment provenance, we first define oxic baseline values for the Welsh Basin, utilizing deeper water, well-oxygenated intervals of late Llandovery age. Our approach documents unstable, oscillating redox conditions on the mid-shelf at Buttington. We suggest that these dynamic redox fluctuations are likely to relate to changes in the position of the chemocline or a migrating oxygen minimum zone. Benthic biota, such as trilobites, brachiopods, bivalves and gastropods, appear to have been relatively unaffected by fluctuating oxic-ferruginous conditions, but were more severely impacted by the development of euxinia, highlighting the inhibiting role of toxic sulfides. By contrast, the redox perturbations appear to have placed extreme stress on graptolites, causing many extinction losses regardless of the specific development of euxinia.

Supplementary material: The geochemical data for the Buttington section is available at https://doi.org/10.6084/m9.figshare.c.7165009

Thematic collection: This article is part of the Chemical Evolution of the Mid-Paleozoic Earth System and Biotic Response collection available at: https://www.lyellcollection.org/topic/collections/chemical-evolution-of-the-mid-paleozoic-earth-system

Received 14 September 2023; **revised** 5 February 2024; **accepted** 13 March 2024

The Llandovery–Wenlock boundary of the early Silurian is marked by both marine environmental changes and biotic turnover (Calner 2008; Lehnert *et al.* 2010; Loydell and Large 2019). The Ireviken Extinction Event (IEE), which was a crisis interval for conodonts, chitinozoans, trilobites and brachiopods (Jeppsson 1997; Jeppsson *et al.* 1998; Hints *et al.* 2006), straddles this boundary and coincides with the onset of a substantial positive isotope excursion in both carbonate ($\delta^{13}C_{carb}$) and organic carbon ($\delta^{13}C_{org}$), termed the Early Sheinwoodian Carbon Isotope Excursion (ESCIE) (Saltzman 2001; Munnecke *et al.* 2003; Cramer *et al.* 2012; Oborny *et al.* 2020; Hartke *et al.* 2021). The start of the ESCIE can be dated to the late *murchisoni* graptolite Biozone (Figs 1, 2; Kaljo and Martma 2006; Loydell and Frýda 2007). Values then peak around the *riccartonensis* Biozone, before the excursion ends in the mid-Sheinwoodian (Fig. 2), during the *belophorus* (formerly *flexilis*) Biozone (Loydell and Frýda 2007). The ESCIE has been attributed to the enhanced burial of organic carbon in anoxic deep ocean and intra-cratonic basinal settings at a time when there was an expansion of carbonate platforms in lower latitude epeiric seas (Jeppsson 1990; Bickert *et al.* 1997; Cramer and Saltzman 2007).

Hypoxia-triggered marine extinctions and carbon cycle perturbations appear to have been a recurring scenario during the Silurian (Jeppsson *et al.* 1998; Calner 2008; Young *et al.* 2020) and a recent study in the Baltic region has shown that the early Sheinwoodian saw the expansion of euxinia (sulfidic water column conditions) in a continental margin location, with potential consequences for the resident biota (Young *et al.* 2019). Although both the IEE and ESCIE are observed globally, potential sulfur isotope (e.g. carbonate-associated sulfate ($\delta^{34}S_{CAS}$) and pyrite sulfur ($\delta^{34}S_{py}$) isotopes) evidence for widespread shelf euxinia (Rose *et al.* 2019; Richardson *et al.* 2021) has been questioned based on a suggested dominant control of lithofacies variability on isotope compositions due to regional sea-level change (Pasquier *et al.* 2021). In this scenario, observed increases in sulfur isotope compositions may have been a consequence of enhanced closed system diagenesis as the local sedimentation rate varied, rather than being due to elevated water column $\delta^{34}S$ compositions through sulfate drawdown under widespread euxinic conditions. Furthermore, most studies have concentrated on shallow water carbonate platforms (Jeppsson 1997; Munnecke *et al.* 2003; Lehnert *et al.* 2010; Hughes and Ray 2016; Yan *et al.* 2022), while the redox state of deeper siliciclastic successions remains more poorly constrained.

Here, we report a reconstruction of the redox history of the early Wenlock (Sheinwoodian) interval from a mid-shelf section in the Welsh Basin (Fig. 1) using a combination of iron speciation and redox-sensitive trace metal systematics. Our focus is on high-resolution, siliciclastic samples from Buttington, east Wales (Loydell and Large 2019). However, because baseline oxic geochemical values can vary between basins, we also assessed samples from two deeper water sections within the Welsh Basin to characterize the oxic geochemical signature in the region. The Buttington section has been the subject of detailed palaeoecological investigation (Loydell and Large 2019) and thus provides an ideal opportunity to investigate the biotic response of a mid-shelf region to the major environmental perturbations that occurred during the early Wenlock.

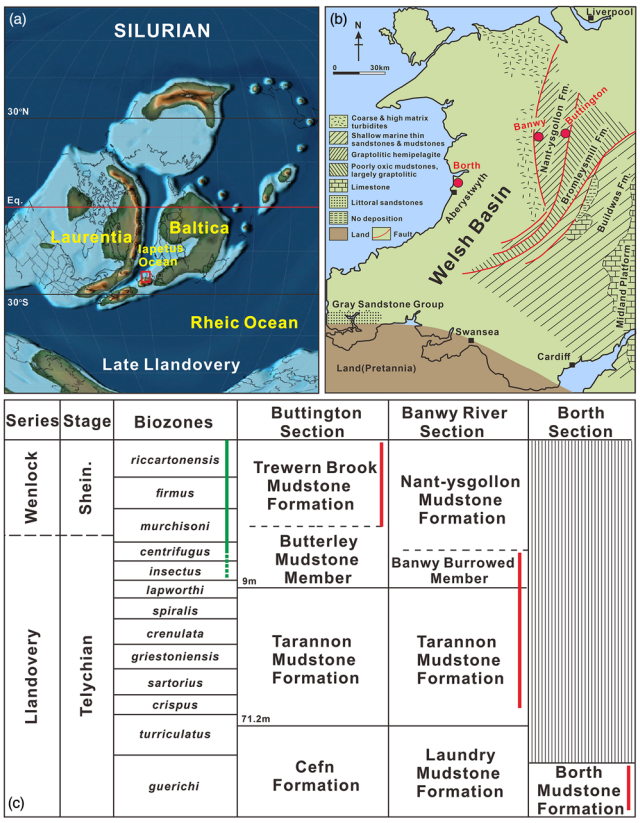

Fig. 1. (**a**) Global palaeogeography of Laurentia and Baltica in the late Llandovery, Silurian, with the red box showing the location of the Welsh Basin. (**b**) Palaeogeography of the Welsh Basin during the *riccartonensis* Biozone (mid-Sheinwoodian). (**c**) Stratigraphic correlation between the study sections. The red lines represent the sampled zones and the green line represents the duration of the Ireviken Extinction Event, with the dashes representing uncertainty in the precise timing of the onset of this event. Source: part (a) modified from Scotese (2014); part (b) modified from Loydell and Cave (1996); part (c) after Loydell and Cave (1996).

Study area and sampled sections

The Ordovician–Silurian Welsh Basin records deposition on the northerly facing margin of the Avalonia microcontinent and has the Midland Platform of central England on its eastern margin (James 2005; Fig. 1a). The microcontinent drifted northwards as the Iapetus Ocean subducted beneath the Laurentia continent and, by the early Silurian, the ocean had narrowed considerably (Stone 2014). Our focus is on three lower Silurian mudstone-dominated sections from the basin centre (Borth section), deep outer shelf (River Banwy section) and mid-shelf (Buttington section) (Fig. 1b). The Borth section (Fig. 1c) is of early Telychian (late Llandovery) age (i.e. prior to the onset of the IEE and ESCIE) and records a mudstone-dominated turbidite succession developed distal to the turbiditic sandstones of the Aberystwyth Grits (Baker and Baas 2020). The River Banwy location comprises a continuous mudstone-dominated section spanning much of the Llandovery–lower Wenlock (Fig. 1c; Loydell and Frýda 2007). We utilize the Borth and Banwy sections to provide regional baseline oxic values for consideration of redox proxy data from the key Buttington section because such data may be particularly basin-specific (Algeo and Li 2020; Poulton 2021; Li *et al.* 2024). Hence, for the Banwy River section, our focus is only on samples from the upper *crispus* to lower *centrifugus* graptolite biozones, prior to the onset of the IEE and ESCIE (Fig. 1c).

The Buttington section consists of early Silurian strata, including most of the Telychian Stage and the lower part of the Sheinwoodian Stage (Fig. 1c). The lower Cefn Formation consists of interbedded tempestite sandstones and mudstones (Loydell and Cave 1993) that unconformably overlie Ordovician shales (Fig. 3). The overlying Tarannon Mudstone Formation predominantly consists of green and purple shale. The Trewern Brook Formation is a dark grey mudstone with an 8.75 m thick olive calcareous silty mudstone unit at its base (Butterley Mudstone Member) and several thin bentonites (Fig. 3; Cave and Dixon 1993; Loydell and Cave 1993). Our focus is on the upper *murchisoni* to *riccartonensis* biozones of the Sheinwoodian Stage, which were sampled in an active quarry (Buttington) near Welshpool in Powys, Wales. Previous research has established a detailed graptolite record and carbon isotope chemostratigraphy for this section, demonstrating that the samples correspond to the early part of the ESCIE and the onset of the peak part of the IEE (Loydell *et al.* 2014; Loydell and Large 2019).

Materials and methods

Samples

High-resolution sampling was conducted at Buttington, with 120 samples of dark grey mudstone collected from a 12.5 m thick section from the uppermost Butterley Mudstone Member (lower Sheinwoodian) and continuing into the lower Trewern Brook Formation (Fig. 3). From the Banwy River section, ten samples of light grey mudstones from the Telychian *crispus* to *centrifugus* biozones were analysed, while for the coastal cliff section at Borth (see Cave and Loydell 1997; James 2005), 78 pale grey mudstones from the early Telychian *guerichi* Biozone of the Borth Mudstones Formation were analysed (Fig. 1c). All samples underwent careful removal of weathered surfaces prior to analysis.

Total organic carbon

For the determination of total organic carbon (TOC), sample powders were pretreated with 10% HCl and shaken overnight twice to remove carbonate phases. The residues were then washed at least three times with Milli-Q water to eliminate residual acid. Dried and powdered samples were analysed on a LECO CS-230 carbon/sulfur analyser. Replicate analyses of certified standards (Soil 502–309, $n = 16$) gave a relative standard deviation (RSD) of <3% and the measurements were within 2% of the certified values.

Iron speciation

Iron speciation was determined via an operationally defined sequential extraction scheme for unsulfidized phases (Poulton and Canfield 2005; Poulton 2021) and a separate extraction scheme for iron sulfides (Canfield *et al.* 1986). These techniques target iron in carbonate phases (Fe_{carb}), iron (oxyhydr)oxides (Fe_{ox}), magnetite iron (Fe_{mag}) and sulfide-bound iron (Fe_{py}), which together comprise highly reactive iron (Fe_{HR}). The Fe_{carb} pool was extracted using sodium acetate solution at pH 4.5 and 50°C for 48 h, followed by treatment with sodium dithionate for 2 h at room temperature to extract Fe_{ox}. The Fe_{mag} pool was then extracted with an ammonium oxalate solution for 6 h at room temperature. Iron concentrations were determined via atomic absorption spectrometry. Replicate analyses ($n = 8$) of international reference material WHIT (Alcott *et al.* 2020) gave an RSD of <5% for all stages and the analyses were within 3% of the certified values. Sulfide-bound iron, including acid-volatile sulfide (Fe_{AVS}; below detection in all instances) and pyrite (Fe_{py}), was extracted using a two-step HCl and $CrCl_2$ technique (Canfield *et al.* 1986). The liberated H_2S was collected as Ag_2S, which was determined gravimetrically and converted stoichiometrically to Fe_{py} concentrations, with an RSD of <5%.

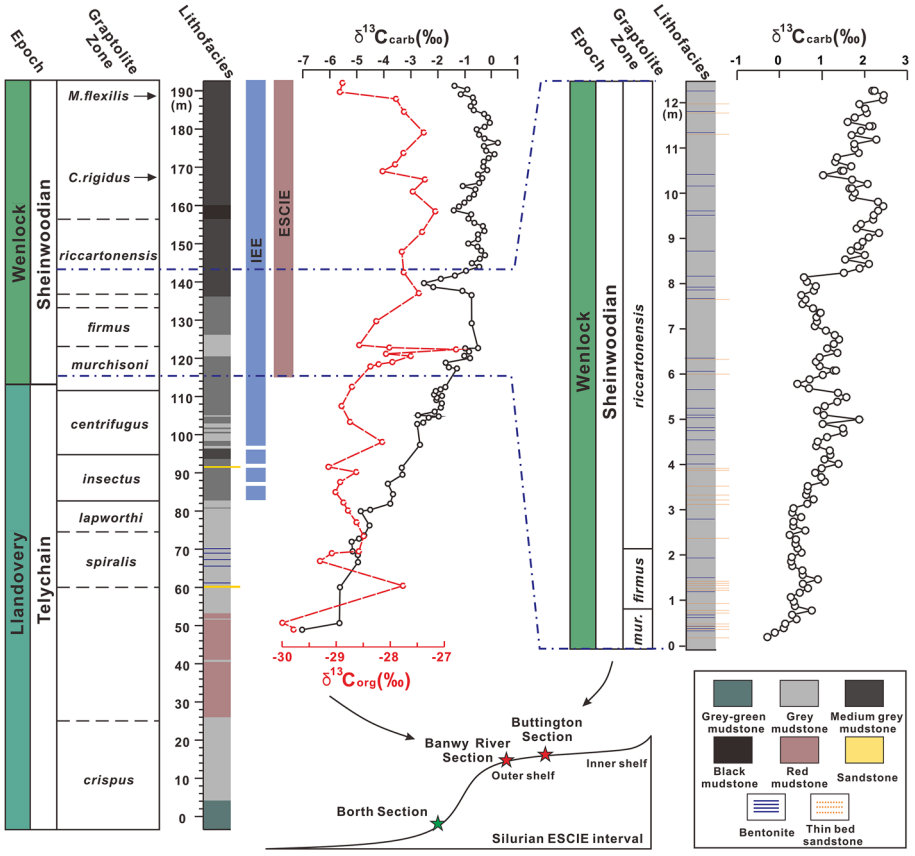

Fig. 2. Correlation of carbon isotope curves at the Buttington and River Banwy sections. Isotope ($\delta^{13}C_{org}$ and $\delta^{13}C_{carb}$) data for the Banwy River section are from Loydell and Frýda (2007) and Cramer *et al.* (2010) and $\delta^{13}C_{carb}$ data for the Buttington section are from Loydell *et al.* (2014). IIE, Ireviken Extinction Event; ESCIE, Early Sheinwoodian Carbon Isotope Excursion.

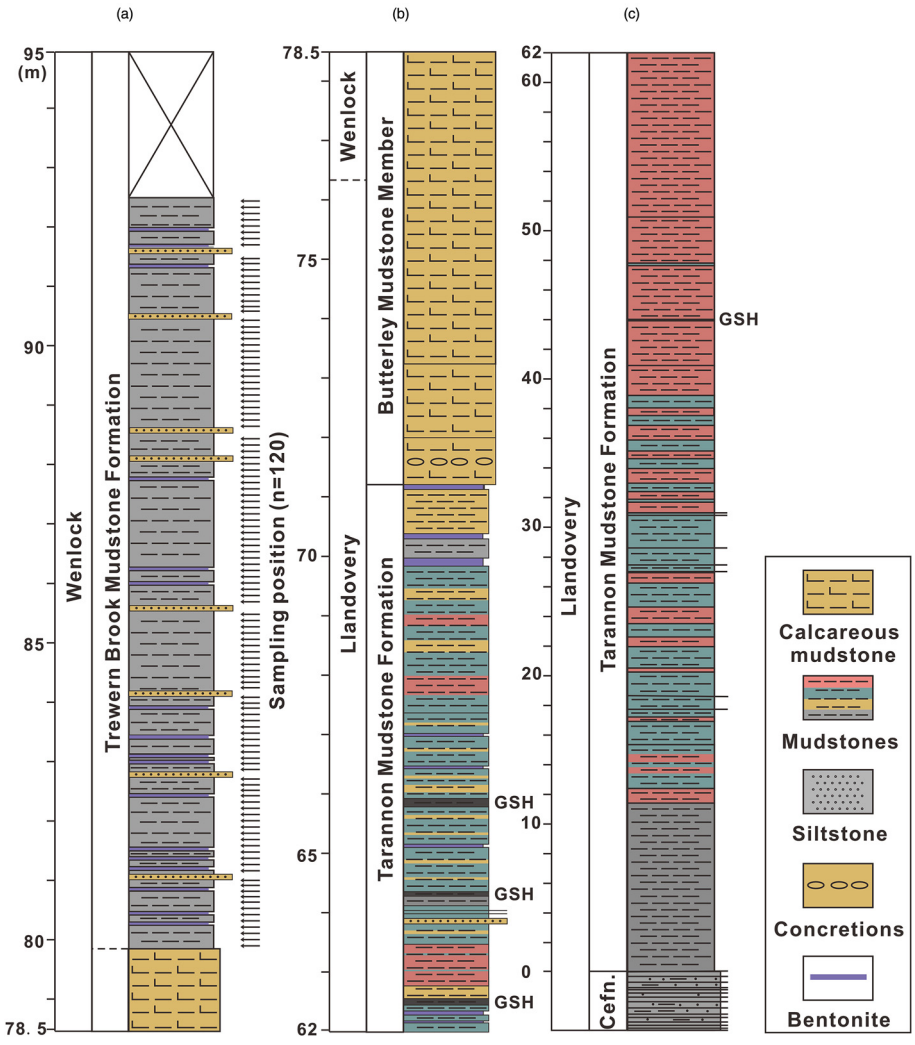

Fig. 3. Detailed lithological logs of the Buttington section. GSH, graptolitic shale horizons. Source: modified from Cave and Dixon (1993) and Loydell and Large (2019).

Bulk element concentrations

About 80 mg of powder were ashed at 550°C for 8 h, followed by dissolution with HNO_3–HF–$HClO_4$. After evaporation to dryness, the samples were treated with H_3BO_3 and heated to dryness again, prior to being re-dissolved with hot HNO_3. Total element concentrations were determined via inductively coupled plasma atomic emission spectrometry (ThermoFisher iCAP 7400) for major elements and inductively coupled plasma mass spectrometry (ThermoFisher iCAPQc) for trace elements. Replicate extractions of international sediment standard SGR-1 yielded RSD values of <2% for all major and trace elements of interest and the analyses were within 3% of the certified values.

Framework for redox interpretations

To reconstruct water column redox conditions, we utilized independent inorganic redox proxies based on iron speciation and redox-sensitive trace metal concentrations. Iron speciation considers the ratio of Fe_{HR} to total iron (Fe_T) (Poulton and Canfield 2005, 2011; Poulton 2021) and extensive calibration in both modern and ancient (which, by definition, considers the effects of diagenesis; cf. Pasquier *et al.* 2022) settings has led to general thresholds to distinguish oxic and anoxic depositional conditions (Raiswell and Canfield 1998; Raiswell *et al.* 2001, 2018; Poulton and Raiswell 2002; Poulton and Canfield 2011; Clarkson *et al.* 2014; Poulton 2021). Oxic water column conditions are commonly indicated when $Fe_{HR}/Fe_T \leq 0.22$, in contrast with ratios ≥ 0.38, which commonly occur due to additional water column precipitation of Fe_{HR} phases under anoxic conditions (Poulton and Canfield 2005). Intermediate Fe_{HR}/Fe_T ratios (between 0.22 and 0.38) are considered equivocal (Poulton and Canfield 2011) and additional evidence for water column redox conditions should be considered in these instances. In addition, however, an independent calibration of redox proxy thresholds should be considered for the particular study area where possible (Algeo and Li 2020; Poulton 2021) and thus we utilized this approach to provide an oxic Fe_{HR}/Fe_T range for the Welsh Basin.

For anoxic samples, the ratio Fe_{py}/Fe_{HR} can be used to distinguish between euxinic and ferruginous settings, whereby ratios >0.6–0.8 commonly indicate euxinia (Anderson 2004; März *et al.* 2008; Benkovitz *et al.* 2020) and ratios $\leq$0.6 imply ferruginous conditions (Poulton and Canfield 2011; Poulton 2021). Intermediate Fe_{HR}/Fe_T ratios (between 0.22 and 0.38) are considered equivocal between oxic and anoxic conditions (Poulton and Canfield 2011), and additional evidence for water column redox conditions should be considered in this case. In addition, however, an independent calibration of redox proxy thresholds should be considered for the particular study area where possible (Algeo and Li 2020; Poulton 2021), and thus we utilized this approach to provide an oxic Fe_{HR}/Fe_T range for the Welsh Basin (see below).

We also note here recent challenges to the use of iron speciation as a palaeo-redox proxy (Pasquier *et al.* 2022). Particular care needs to be taken when iron speciation is applied to sediments with low iron contents (<0.5 wt% Fe_T; Clarkson *et al.* 2014), sediments resulting from rapid deposition (e.g. turbidites; Canfield *et al.* 1996) and those in proximity to hydrothermal inputs (Raiswell *et al.* 2018) or directly adjacent to (sub)tropical mountainous regions, where highly weathered sediments may supply a high proportion of Fe_{HR} directly onto the continental margin (Wei *et al.* 2021), thus circumventing the preferential trapping of Fe_{HR} that usually occurs in nearshore environments (Poulton and Raiswell 2002). However, our calibration of regional oxic baseline values circumvents these potential problems and our combined approach of using independent redox-sensitive trace metal (specifically uranium, molybdenum and rhenium) systematics provides a particularly robust assessment of the chemical conditions of deposition (Poulton 2021).

Uranium and molybdenum are highly soluble and exhibit limited enrichment in oxic sediments (Morford *et al.* 2009). Uranium predominantly exists as U^{VI} in uranyl carbonate complexes ($UO_2(CO_3)_3^{4-}$) in oxic seawater (Calvert and Pedersen 1993), whereas molybdenum is stable as Mo^{VI} in the molybdate oxyanion (MoO_4^{2-}) under such conditions (Zheng *et al.* 2000). When anoxia develops around the sediment–water interface, soluble U^{VI} is reduced to insoluble U^{IV}, primarily at the onset of the Fe^{II}–Fe^{III} redox boundary (Anderson *et al.* 1989). By contrast, the removal of molybdenum requires the specific presence of relatively high concentrations of HS^- in the water column, resulting in the formation of thiomolybdates ($MoO_xS_4^{x-}$) under euxinic conditions (Helz *et al.* 1996; Zheng *et al.* 2002). Rhenium is enriched in sediments located just below the sediment–water interface (*c.* 1 cm), even under weakly reducing (dysoxic) conditions that lack uranium and molybdenum enrichment (Crusius *et al.* 1996).

Thus, the combined consideration of rhenium, uranium and molybdenum systematics, alongside iron speciation, may allow dysoxic, anoxic non-sulfidic (ferruginous) and euxinic conditions to be distinguished. However, oxic baseline values for redox-sensitive trace metals are particularly basin-specific (Algeo and Li 2020) because there is a strong dependence on the composition of the sediment supplied to the basin. Therefore, as with the Fe_{HR}/Fe_T ratios, we utilize oxic samples from the basin to calibrate baseline depositional values for rhenium, uranium and molybdenum, thus allowing redox-driven enrichments to be fully assessed.

Results

In the Borth and Banwy River sections, TOC ranges from 0.11 to 0.28 wt%, with an average of 0.18 ± 0.03 wt% (Fig. 4). In the Buttington section, the TOC values are generally higher, ranging from 0.19 to 0.68 wt%, with an average of 0.39 ± 0.03 wt% (Figs 4, 5a). Although the data show scatter, there are distinct zones that generally have higher TOC concentrations (up to 0.6–0.7 wt%; Fig. 5a).

The phase partitioning of iron is relatively constant in the Buttington section (Fig. 5d) and is dominated by reduced iron phases (Fe_{carb}, Fe_{mag} and Fe_{py}), with oxidized phases (Fe_{ox}) accounting for only 7.6 ± 4.2% of the total Fe_{HR} pool. The Fe_{HR}/Fe_T ratios average 0.40 ± 0.08 and the Fe_{py}/Fe_{HR} ratios average 0.40 ± 0.11 (Fig. 4), with both ratios showing little systematic variation up-section (Fig. 5). By contrast, the Fe_{HR}/Fe_T ratios are consistently lower in the Banwy River (average 0.08 ± 0.03) and Borth (average 0.08 ± 0.02) sections, while the Fe_{py}/Fe_{HR} ratios are also very low (Banwy River, 0.03 ± 0.02; Borth, 0.08 ± 0.14; Fig. 4).

The average U/Al and Mo/Al ratios for all three sections fall below the average upper continental crust (UCC) compositions (Fig. 4), with the Buttington section having distinctly higher values (U/Al = 0.32 ± 0.04; Mo/Al = 0.13 ± 0.08) than the Banwy River (U/Al = 0.22 ± 0.05; Mo/Al = 0.02 ± 0.01) and Borth (U/Al = 0.22 ± 0.02; Mo/Al = 0.06 ± 0.06) sections (Fig. 4). By contrast, the Re/Al ratios are slightly above the UCC value for the Banwy River (0.12 ± 0.03) and Borth (0.10 ± 0.02) sections, but these ratios are again considerably higher in the Buttington section (0.35 ± 0.10; Fig. 4). Through the Buttington section, the U/Al ratios are relatively stable (Fig. 5e), whereas the Mo/Al ratios show considerable fluctuations, with five clear intervals of higher values (Fig. 5f). The Re/Al ratios are relatively stable in the lower part of the section, but show more variability up-section, although there is no consistent trend in the data (Fig. 5g).

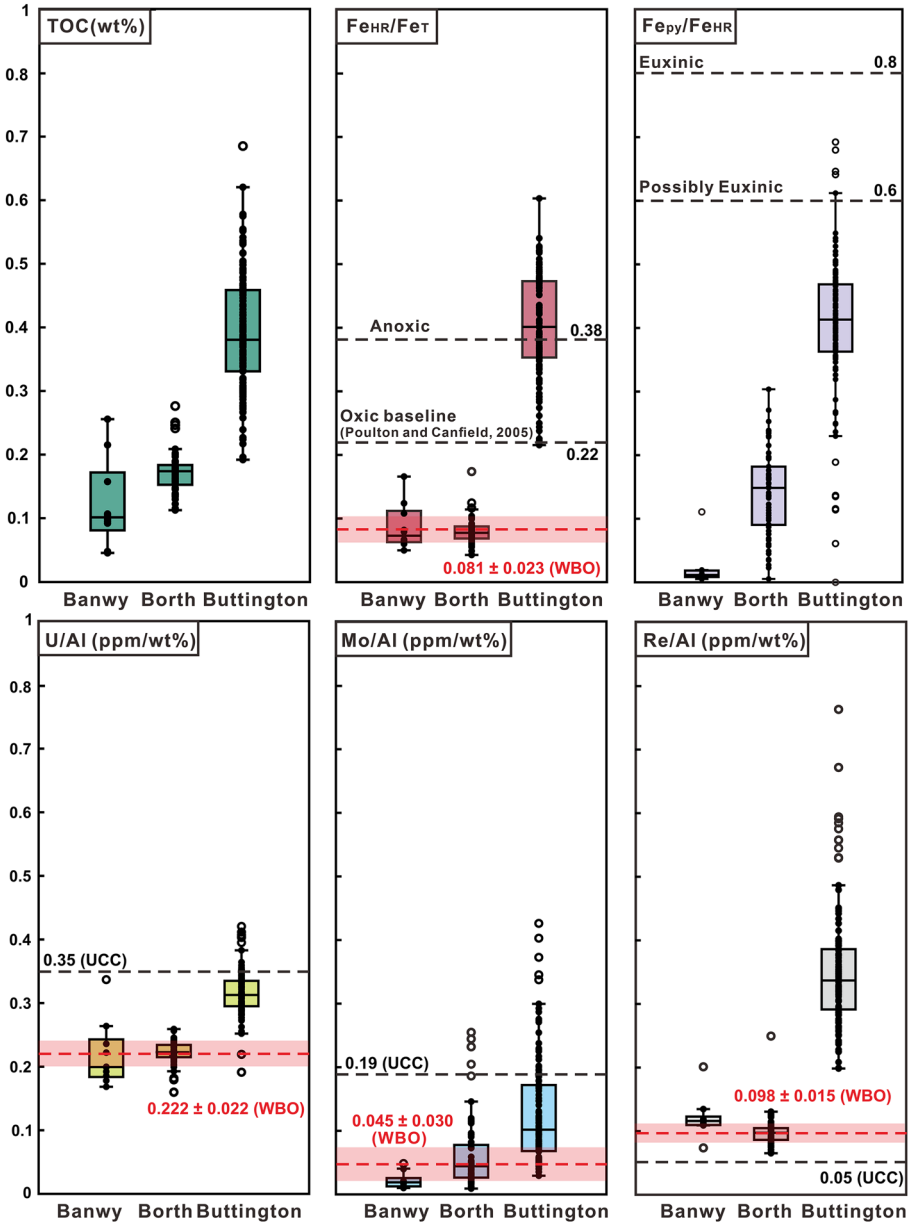

Fig. 4. Total organic carbon, redox proxy data and oxic baseline establishment for the early Silurian Welsh Basin. Boxes represent the interquartile range and whiskers represent 1σ. The lines labelled WBO represent the Welsh Basin Oxic values or ranges for the early Silurian. Specifically, shading on the Fe_{HR}/Fe_T plot represents the WBO oxic baseline range for the Borth and Banwy River sections and the red dashed lines and shading on the redox-sensitive trace metal plots represent the average oxic values and the 1σ range, respectively. UCC, upper continental crust, referred from Mclennan (2001).

Discussion

Establishing an oxic baseline for the Welsh Basin

Whenever possible, redox interpretations should be calibrated for the specific site of interest because general redox thresholds are often inadequate when applied on a local or regional scale (Algeo and Li 2020; Poulton 2021; Takahashi *et al.* 2021; Li *et al.* 2024). This is clearly the case in the Welsh Basin, where samples from the Banwy River and Borth sections have Fe_{HR}/Fe_T ratios that fall well below the general oxic baseline value (Poulton and Canfield 2011), while the U/Al and Mo/Al ratios are considerably lower than the UCC values (Fig. 4). In addition, the Re/Al ratios are only slightly elevated in the Banwy River and Borth sections, relative to the UCC values, and the extent of pyritization (Fe_{py}/Fe_{HR}) is also very low (Fig. 4). These combined geochemical characteristics strongly suggest deposition under oxic bottom water conditions (Tribovillard *et al.* 2006; Poulton and Canfield 2011), with the slight enrichment in the Re/Al ratios possibly indicating suboxic conditions close to the sediment–water interface. Since there is no evidence for a significant change in the sedimentary provenance on the depositional timescale of these sections (Ball *et al.* 1992), the Banwy River and Borth sections allow oxic baseline values to be defined, here termed the Welsh Basin Oxic (WBO) values (see Fig. 4). For the Fe_{HR}/Fe_T ratios, the oxic baseline for the Welsh Basin was determined as the range measured for the Borth and Banwy River sections, while for redox-sensitive trace metals, the oxic baseline was determined as the average values for the Borth and Banwy River sections (±1σ).

Redox dynamics on the mid-shelf

The enrichments in rhenium (relative to the WBO values) that are apparent throughout the Buttington section (Fig. 5g) suggest that the sediment–water interface was at least dysoxic. In addition, however, the highly elevated Fe_{HR}/Fe_T and U/Al ratios (Fig. 5) suggest that the bottom water conditions were, at least periodically, fully anoxic. This consistent behaviour between independent redox proxies provides support for robust palaeo-redox interpretations. However, the Buttington section is also characterized by varying degrees of bioturbation (see Fig. 6 and later discussion), suggesting that the bottom waters likely fluctuated between fully anoxic and (at least partially) oxic on short timescales. Bioturbation impacts the geochemical record of sediments affected by fluctuating redox conditions by homogenizing anoxic enrichments in Fe_{HR} and redox-

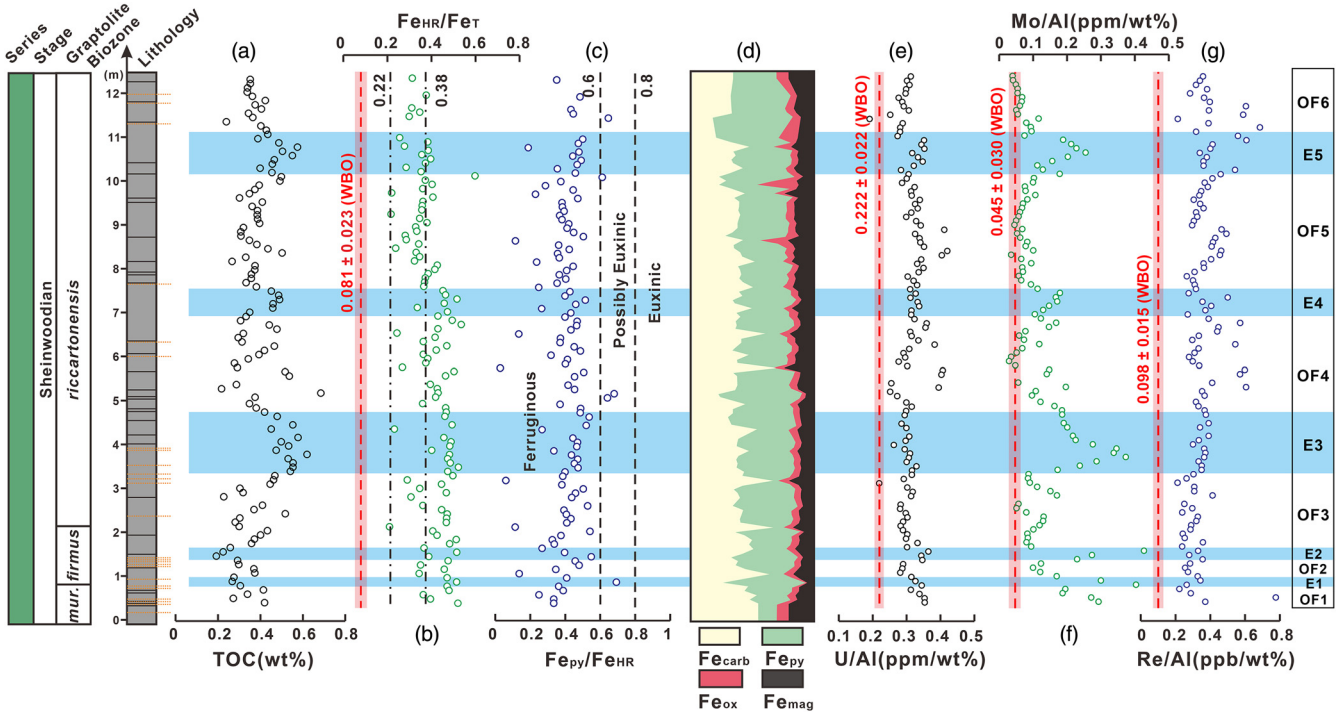

Fig. 5. Geochemical data for the Buttington section of the Trewern Brook Mudstone Formation. Shading on the Fe_{HR}/Fe_T plot represents the Welsh basin oxic baseline range, while the dashed lines on the redox-sensitive trace metal plots represent the Welsh Basin Oxic composition. On the Fe_{HR}/Fe_T plot, published thresholds for general identification of oxic, possibly anoxic and anoxic water column conditions (Poulton and Canfield 2011) are included for context. However, in this instance, these thresholds are superseded by our regional oxic baseline calibration. Dashed lines on the Fe_{py}/Fe_{HR} plot represent calibrated thresholds for the identification of ferruginous, possibly euxinic, and euxinic depositional conditions for anoxic samples (Poulton and Canfield 2011; Poulton 2021). The pale blue shading indicates intervals of more reducing conditions (possibly euxinic). *mur.* = *murchisoni*; WBO, Welsh basin oxic.

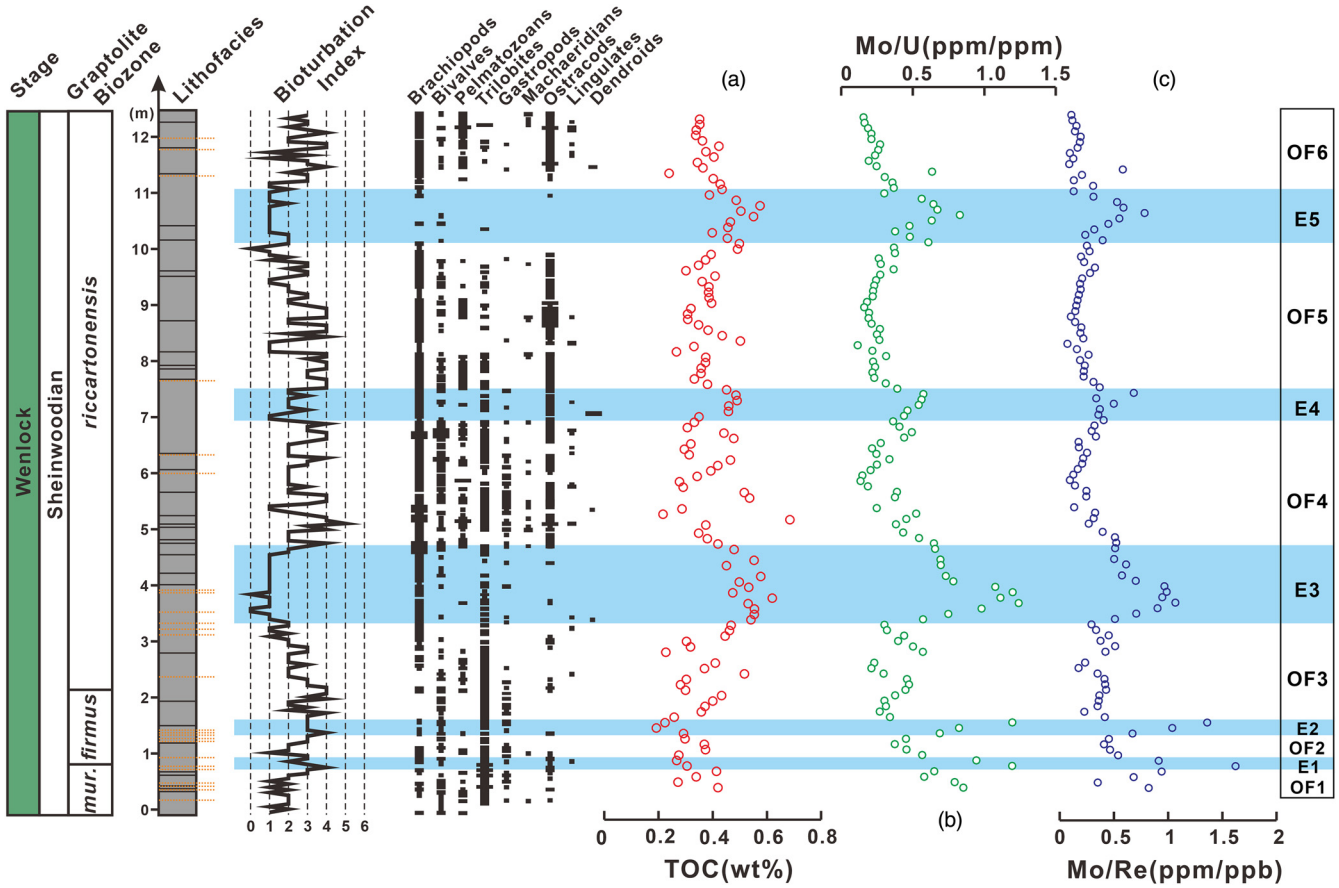

Fig. 6. Palaeoecological data in the context of total organic carbon concentrations and fluctuations in dissolved sulfide in the water column (indicated by Mo/U and Mo/Re ratios). Bioturbation index and the occurrences of common benthic fossil groups (narrow bar, rare; widest bar, very common) are from Loydell and Large (2019).

sensitive trace metals over the depth interval affected by burrowing (Sperling *et al.* 2016; Poulton 2021). Persistent enrichments in both Fe_{HR} and uranium in sediments that have experienced bioturbation therefore point to repetitive fluctuations between oxic/dysoxic and anoxic bottom water conditions (Poulton 2021).

In the Buttington section, the Fe_{py}/Fe_{HR} ratios below the lower threshold (0.6) for recognition of euxinia (Fig. 5c) suggest dominantly ferruginous conditions when the water column was anoxic. However, care should be taken with this interpretation in bioturbated sediments because the introduction of oxygen into sediment porewaters by the action of bioturbation would re-oxidize sulfide phases, likely resulting in decreased Fe_{py}/Fe_{HR} ratios. In this context, the Mo/Al ratios can be used as supporting evidence for the redox state of the water column due to the requirement for relatively high concentrations of free sulfide to convert soluble molybdate to particle-reactive thiomolybdate (Helz *et al.* 1996; Zheng *et al.* 2002). This tends to produce relatively high sediment enrichments in molybdenum, but needs to be considered alongside the caveat that molybdenum enrichments may also occur under ferruginous conditions via a particle shuttle mechanism. In this scenario, molybdenum may be drawn down via adsorption to iron (oxyhydr) oxide minerals precipitated in the ferruginous water column, which generally gives moderate sediment enrichments (e.g. Algeo and Tribovillard 2009; Tribovillard *et al.* 2012).

Our data show several repetitive intervals of increased enrichments in molybdenum (Fig. 5f), despite the potential for the subsequent remobilization and loss of molybdenum from the sediment during short-lived oxic interludes when intense bioturbation occurred (see later). To resolve whether these enrichments reflect drawdown under dominantly euxinic conditions or drawdown via a particulate shuttle mechanism under dominantly ferruginous conditions, a cross-plot of U_{EF} v. Mo_{EF} (where EF represents the enrichment factor of a particular element) is commonly used (Fig. 7; Algeo and Tribovillard 2009; Tribovillard *et al.* 2012). Enrichment factors are normally calculated relative to the average continental crust (e.g. UCC), but, for our samples, where we have demonstrated that the average continental crust does not adequately reflect the composition of the terrestrial sediments delivered to the basin, we instead utilize our average WBO data. Thus we calculate EF values as $element_{EF} = (element/Al)_{sample}/(element/Al)_{WBO}$.

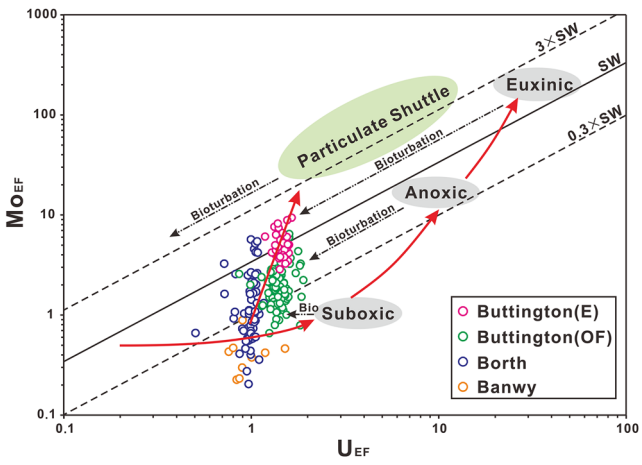

Fig. 7. Plot of Mo_{EF} v. U_{EF} for samples from the Welsh Basin considered in comparison with modern seawater (Algeo and Tribovillard 2009; Tribovillard *et al.* 2012). The impact of bioturbation on the suboxic, anoxic (i.e. ferruginous), euxinic and particulate shuttle zones is shown as dashed lines. The Buttington data are distinguished in terms of the broad intervals identified as being dominantly euxinic (ButtingtonE) and oxic-ferruginous (ButtingtonOF) based on molybdenum systematics (see Fig. 5).

Figure 7 shows that the data plot on a trajectory indicative of a progressive increase in the intensity of reducing conditions (Algeo and Tribovillard 2009; Tribovillard *et al.* 2012). However, the data do not plot in the normal oxic through to euxinic phase space for marine sediments, likely because the impact of bioturbation also needs to be considered. In this context, both uranium and molybdenum would be increasingly remobilized from the sediments as bioturbation intensity increases due to the introduction of oxygenated seawater and the reoxidation of a proportion of the uranium and molybdenum that was originally sequestered as reduced authigenic phases. Therefore, we also consider the basic trajectories that bioturbation would impose on the broad position of the different redox and particulate shuttle zones (see Fig. 7).

Our approach clearly demonstrates that the Buttington data reflect changes in the intensity of reducing conditions (Fig. 7), with intervals where fluctuations between oxic and ferruginous conditions occurred on short timescales (which we term intervals OF1–OF6; Fig. 5). These intervals were, however, separated by periods where the lower water column was likely dominantly euxinic (intervals E1–E5; Fig. 5). As highlighted earlier, these dominantly euxinic intervals (as identified by molybdenum enrichments) do not coincide with the Fe_{py}/Fe_{HR} enrichments indicative of euxinia (Fig. 5), likely due to the partial reoxidation of pyrite during short-lived oxic intervals. Burrowing during these oxic intervals only produced bioturbation indices in the range 1–3 (Fig. 6), although small-scale burrowing by meiofauna could also have contributed without causing visible burrows. However, during bioturbation, anoxic Fe_{HR}/Fe_T enrichments would have been preserved due to the immediate re-precipitation of pyrite iron as (oxyhydr)oxide phases. Thus the combined geochemical signals are entirely consistent with intervals where deposition dominantly occurred under euxinic conditions, but with short-lived periods of better oxygenated conditions promoting limited bioturbation of the sediments (see Fig. 6). This dichotomy between geochemical proxies that record long-term redox conditions and palaeoecological data that record short-term, better oxygenated interludes, is often encountered in ancient redox studies (e.g. Wignall 1994).

Redox controls on the benthic biota and cause of the IEE

Bioturbation intensity varies considerably at Buttington (Loydell and Large 2019), with several intervals also being characterized by relatively low biotic diversity (Fig. 6). To investigate the potential roles of anoxia and sulfide toxicity on the biota, we recast the geochemical data in terms of the Mo/U and Mo/Re ratios (Fig. 6), whereby high values denote elevated availability of dissolved sulfide in the water column and during early diagenesis. The euxinic intervals E3 and E5 and, to a lesser extent, E4, correspond with intervals of low bioturbation intensity and very low benthic diversity at times of prolonged euxinia (Fig. 6). By contrast, the first two shorter lived euxinic intervals (E1 and E2) show little distinct impact in terms of either bioturbation intensity or benthic diversity. This may be because the ecosystem was placed under progressive strain by each subsequent interval of euxinia, leading to increasingly detrimental consequences for the biota or, alternatively, the timescale of each euxinic pulse may have been critical, with longer intervals having a more pronounced impact. In this latter context, we also note that the sediment deposited during the first two shorter euxinic pulses would mostly have been within the potential bioturbation depth zone when the system recovered from euxinia. Hence, for these shorter euxinic pulses, the bioturbation index and benthic diversity parameters may have been overprinted by subsequent bioturbation when the system recovered to a more amenable oxic-ferruginous state.

In addition, some of the fluctuating oxic-ferruginous intervals (particularly OF2, OF3, OF5 and OF6) are also characterized by

relatively low diversity (but not to the extent of the euxinic intervals), although the bioturbation intensity appears to be largely unaffected (Fig. 6). We speculate that variability in the biotic response during these oxic-ferruginous intervals may reflect changes in the relative persistence of oxic v. anoxic conditions, with intervals of relatively prolonged or more frequent oxygenation promoting increased diversity.

Overall, the consistent lithofacies throughout the Buttington section suggests that the benthic fauna likely experienced uniform substrate conditions. As a result, variations in bioturbation activity were likely more influenced by changes in the redox conditions than substrate consistency, with euxinia exerting a particularly strong impact. Benthic faunas demonstrate distinct evolutionary behaviours in response to varying oxygenation levels (Wignall 1990). At Buttington, several benthic groups, including trilobites, brachiopods, bivalves and gastropods, were relatively unaffected during the oxic-ferruginous intervals (Fig. 6). By contrast, survival of the benthos was more challenging in the dominantly euxinic intervals (Fig. 6).

Our analysis of the Buttington section reveals dynamic, high-amplitude redox changes in this mid-shelf setting during an interval that marks the early stages of the IEE, immediately before and during the onset of the ESCIE (Fig. 2). The extinction interval was characterized by a graptolite crisis, which persisted until the early *riccartonensis* Zone (Loydell and Large 2019). The graptolite losses therefore correspond to the highly variable redox conditions at Buttington, but it remains to be seen if these variations are repeated in other regions and locations. It is notable, however, that the earlier major graptolite extinction that occurred during the first phase of the end-Ordovician mass extinction (at the end of the Katian Stage) has also been ascribed to rapid redox variations, rather than persistent anoxia (Kozik *et al.* 2022). It therefore appears likely that the dynamic fluctuations in marine redox conditions observed at Buttington may have had a significant role in the biotic crisis during the early Sheinwoodian Stage of the Silurian.

A broader scale oceanic anoxic event has been proposed for this time interval (Emsbo *et al.* 2010), which may have been triggered by a substantial increase in primary production (Young *et al.* 2019; Cichon-Pupienis *et al.* 2021), while an alternative hypothesis involves a marine sedimentary–exhalative brine event (Emsbo 2017). Our data provide little direct insight into the primary driver(s) of anoxia at this time. However, both the broader scale redox fluctuations between ferruginous and euxinic conditions, and the shorter term transitions to better oxygenated conditions, likely reflect changes in the position of the chemocline, or a migrating oxygen minimum zone, highlighting that the redox conditions were highly unstable, at least in the mid-shelf locations. Indeed, the Mo/Al ratios suggest a degree of cyclicity in the data (particularly if the two shorter euxinic intervals towards the base of the section are considered as one broader interval) and we note that these euxinic intervals commonly occur coincident with the zones that generally have higher TOC concentrations (Fig. 5). This potential cyclicity hints at a possible orbital control on the broader scale redox fluctuations, but at present this remains speculative and requires further detailed study.

Conclusions

Our independent redox proxy data from two deep water sections in the Welsh Basin, UK provide oxic baseline values for this trace-metal-lean region during the early Silurian. These calibrations allow a detailed evaluation of water column redox conditions in a mid-shelf location at Buttington. We identify an oscillating redox state on the mid-shelf in the early Wenlock, with extended intervals that were characterized by oxic-ferruginous conditions, but with regular transitions to a dominantly euxinic state. Benthos, such as trilobites, brachiopods, bivalves and gastropods, were relatively unaffected during oxic-ferruginous intervals, although the relative intensity of oxic v. ferruginous conditions appears to have been important. These faunas were, however, substantially impacted by the development of euxinia, highlighting the specific role of toxic hydrogen sulfide as a key factor, on top of the detrimental impact of deoxygenation. Graptolites suffered an extinction crisis at this time, which may have been caused by the difficulties of adaptation to conditions of rapid water column redox variations, although this idea requires investigation of the redox stability in other regions. However, we note that the main end-Ordovician graptolite extinction event also occurred during an interval of dynamic oceanic redox fluctuations (Kozik *et al.* 2022).

In summary, our data contribute to a growing geochemical database on the evolution of ocean redox conditions during the early Silurian and suggest that dynamic fluctuations in regional redox conditions occurred in shelf seas. We thus provide new insights into the nature of more widespread anoxia at this time, as well as the ensuing implications for the biotic record during the IEE.

Scientific editing by Zhongqiang Chen

Acknowledgements We thank Anthony Butcher, Bob Loveridge, Thomas Wignall and Bethany Smith for their help with sample collection.

Author contributions **YW**: conceptualization (lead), data curation (lead), writing – original draft (lead); **PBW**: conceptualization (lead), writing – review and editing (lead); **YX**: methodology (equal); **DKL**: resources (lead); **JP**: investigation (equal); **JHB**: writing – review and editing (supporting); **BJWM**: software (lead); **SWP**: conceptualization (lead), project administration (lead), writing – review and editing (lead).

Funding This study was funded by a University of Leeds research training grant 35009501 (YW) and Natural Environment Research Council grant NE/T008458/1 (SWP).

Competing interests The authors declare that they have no known competing financial interests or personal relationships that could have appeared to influence the work reported in this paper.

Data availability All data generated or analysed during this study are included in this published article (and if present, its supplementary information files).

References

Alcott, L.J., Krause, A.J. *et al.* 2020. Development of iron speciation reference materials for palaeoredox analysis. *Geostandards and Geoanalytical Research*, **44**, 581–591, https://doi.org/10.1111/ggr.12342

Algeo, T.J. and Li, C. 2020. Redox classification and calibration of redox thresholds in sedimentary systems. *Geochimica et Cosmochimica Acta*, **287**, 8–26, https://doi.org/10.1016/j.gca.2020.01.055

Algeo, T.J. and Tribovillard, N. 2009. Environmental analysis of paleoceanographic systems based on molybdenum–uranium covariation. *Chemical Geology*, **268**, 211–225, https://doi.org/10.1016/j.chemgeo.2009.09.001

Anderson, T.F. 2004. Sources and mechanisms for the enrichment of highly reactive iron in euxinic Black Sea sediments. *American Journal of Science*, **304**, 203–233, https://doi.org/10.2475/ajs.304.3.203

Anderson, R., LeHuray, A., Fleisher, M. and Murray, J. 1989. Uranium deposition in Saanich Inlet sediments, Vancouver Island. *Geochimica et Cosmochimica Acta*, **53**, 2205–2213, https://doi.org/10.1016/0016-7037(89)90344-X

Baker, M.L. and Baas, J.H. 2020. Mixed sand–mud bedforms produced by transient turbulent flows in the fringe of submarine fans: indicators of flow transformation. *Sedimentology*, **67**, 2645–2671, https://doi.org/10.1111/sed.12714

Ball, T., Davies, J., Waters, R. and Zalasiewicz, J. 1992. Geochemical discrimination of Silurian mudstones according to depositional process and provenance within the Southern Welsh Basin. *Geological Magazine*, **129**, 567–572, https://doi.org/10.1017/S0016756800021725

Benkovitz, A., Matthews, A., Teutsch, N., Poulton, S.W., Bar-Matthews, M. and Almogi-Labin, A. 2020. Tracing water column euxinia in Eastern

Mediterranean Sapropels S5 and S7. *Chemical Geology*, **545**, 119627, https://doi.org/10.1016/j.chemgeo.2020.119627

Bickert, T., Pätzold, J., Samtleben, C. and Munnecke, A. 1997. Paleoenvironmental changes in the Silurian indicated by stable isotopes in brachiopod shells from Gotland, Sweden. *Geochimica et Cosmochimica Acta*, **61**, 2717–2730, https://doi.org/10.1016/S0016-7037(97)00136-1

Calner, M. 2008. Silurian global events – at the tipping point of climate change. *In*: Elewa, A.M.T. (ed.) *Mass Extinction*. Springer, 21–57, https://doi.org/10.1007/978-3-540-75916-4_4

Calvert, S. and Pedersen, T. 1993. Geochemistry of recent oxic and anoxic marine sediments: implications for the geological record. *Marine Geology*, **113**, 67–88, https://doi.org/10.1016/0025-3227(93)90150-T

Canfield, D.E., Raiswell, R., Westrich, J.T., Reaves, C.M. and Berner, R.A. 1986. The use of chromium reduction in the analysis of reduced inorganic sulfur in sediments and shales. *Chemical Geology*, **54**, 149–155, https://doi.org/10.1016/0009-2541(86)90078-1

Canfield, D.E., Lyons, T.W. and Raiswell, R. 1996. A model for iron deposition to euxinic Black Sea sediments. *American Journal of Science*, **296**, 818–834, https://doi.org/10.2475/ajs.296.7.818

Cave, R. and Dixon, R. 1993. The Ordovician and Silurian of the Welshpool area. *In:* Woodcock, N.H. and Bassett, M.G. (eds) *Geological Excursions in Powys, Central Wales*. Geologists' Association, 51–84.

Cave, R. and Loydell, D.K. 1997. The eastern margin of the Aberystwyth Grits Formation. *Geological Journal*, **32**, 37–44, https://doi.org/10.1002/(SICI)1099-1034(199703)32:1%3C37::AID-GJ717%3E3.0.CO;2-U

Cichon-Pupienis, A., Littke, R., Lazauskienė, J., Baniasad, A., Pupienis, D., Radzevičius, S. and Šiliauskas, L. 2021. Geochemical and sedimentary facies study – implication for driving mechanisms of organic matter enrichment in the lower Silurian fine-grained mudstones in the Baltic Basin (W Lithuania). *International Journal of Coal Geology*, **244**, 103815, https://doi.org/10.1016/j.coal.2021.103815

Clarkson, M.O., Poulton, S.W., Guilbaud, R. and Wood, R.A. 2014. Assessing the utility of Fe/Al and Fe-speciation to record water column redox conditions in carbonate-rich sediments. *Chemical Geology*, **382**, 111–122, https://doi.org/10.1016/j.chemgeo.2014.05.031

Cramer, B.D. and Saltzman, M.R. 2007. Early Silurian paired $\delta^{13}C_{carb}$ and $\delta^{13}C_{org}$ analyses from the Midcontinent of North America: implications for paleoceanography and paleoclimate. *Palaeogeography, Palaeoclimatology, Palaeoecology*, **256**, 195–203, https://doi.org/10.1016/j.palaeo.2007.02.032

Cramer, B.D., Kleffner, M.A., Brett, C.E., McLaughlin, P.I., Jeppsson, L., Munnecke, A. and Samtleben, C. 2010. Paleobiogeography, high-resolution stratigraphy, and the future of Paleozoic biostratigraphy: fine-scale diachroneity of the Wenlock (Silurian) conodont *Kockelella walliseri*. *Palaeogeography, Palaeoclimatology, Palaeoecology*, **294**, 232–241, https://doi.org/10.1016/j.palaeo.2010.01.002

Cramer, B.D., Condon, D.J. *et al.* 2012. U–Pb (zircon) age constraints on the timing and duration of Wenlock (Silurian) paleocommunity collapse and recovery during the 'Big Crisis'. *GSA Bulletin*, **124**, 1841–1857, https://doi.org/10.1130/b30642.1

Crusius, J., Calvert, S., Pedersen, T. and Sage, D. 1996. Rhenium and molybdenum enrichments in sediments as indicators of oxic, suboxic and sulfidic conditions of deposition. *Earth and Planetary Science Letters*, **145**, 65–78, https://doi.org/10.1016/S0012-821X(96)00204-X

Emsbo, P. 2017. Sedex brine expulsions to Paleozoic basins may have changed global marine $^{87}Sr/^{86}Sr$ values, triggered anoxia, and initiated mass extinctions. *Ore Geology Reviews*, **86**, 474–486, https://doi.org/10.1016/j.oregeorev.2017.02.031

Emsbo, P., McLaughlin, P., Munnecke, A., Breit, G., Koenig, A., Jeppsson, L. and Verplanck, P. 2010. The Ireviken event: a Silurian OAE. *Geological Society of America Annual Meeting*, 31 Octover–3 November 2010, Denver, Colorado, Abstracts, **42**, 561.

Hartke, E.R., Cramer, B.D., Calner, M., Melchin, M.J., Barnett, B.A., Oborny, S.C. and Bancroft, A.M. 2021. Decoupling $\delta^{13}C_{carb}$ and $\delta^{13}C_{org}$ at the onset of the Ireviken carbon isotope excursion: $\Delta^{13}C$ and organic carbon burial (f_{org}) during a Silurian oceanic anoxic event. *Global and Planetary Change*, **196**, 103373, https://doi.org/10.1016/j.gloplacha.2020.103373

Helz, G., Miller, C., Charnock, J., Mosselmans, J., Pattrick, R., Garner, C. and Vaughan, D. 1996. Mechanism of molybdenum removal from the sea and its concentration in black shales: EXAFS evidence. *Geochimica et Cosmochimica Acta*, **60**, 3631–3642, https://doi.org/10.1016/0016-7037(96)00195-0

Hints, O., Killinga, M., Männik, P. and Nestor, V. 2006. Frequency patterns of chitinozoans, scolecodonts, and conodonts in the upper Llandovery and lower Wenlock of the Paatsalu core, western Estonia. *Proceedings of the Estonian Academy of Sciences, Geology*, **55**, 128–155, https://doi.org/10.3176/geol.2006.2.04

Hughes, H.E. and Ray, D.C. 2016. The carbon isotope and sequence stratigraphic record of the Sheinwoodian and lower Homerian stages (Silurian) of the Midland Platform, UK. *Palaeogeography, Palaeoclimatology, Palaeoecology*, **445**, 97–114, https://doi.org/10.1016/j.palaeo.2015.12.022

James, D.M.D. 2005. Palaeotopography of the northern portion of the Telychian (Silurian) turbidite basin in central Wales. *Geological Journal*, **40**, 593–601, https://doi.org/10.1002/gj.1028

Jeppsson, L. 1990. An oceanic model for lithological and faunal changes tested on the Silurian record. *Journal of the Geological Society*, **147**, 663–674, https://doi.org/10.1144/gsjgs.147.4.0663

Jeppsson, L. 1997. The anatomy of the mid–early Silurian Ireviken Event. *In*: Brett, C.E. and Baird, G.C. (eds) *Paleontological Events: Stratigraphic, Ecological, and Evolutionary Implications*. Columbia University Press, 451–492.

Jeppsson, L., Landing, E. and Johnson, M.E. 1998. Silurian oceanic events: summary of general characteristics. *New York State Museum Bulletin*, **491**, 239–257.

Kaljo, D. and Martma, T. 2006. Application of carbon isotope stratigraphy to dating the Baltic Silurian rocks. *GFF*, **128**, 123–129, https://doi.org/10.1080/11035890601282123

Kozik, N.P., Young, S.A. *et al.* 2022. Rapid marine oxygen variability: driver of the Late Ordovician mass extinction. *Science Advances*, **8**, eabn8345, https://doi.org/10.1126/sciadv.abn8345

Lehnert, O., Männik, P., Joachimski, M.M., Calner, M. and Frýda, J. 2010. Palaeoclimate perturbations before the Sheinwoodian glaciation: a trigger for extinctions during the 'Ireviken Event'. *Palaeogeography, Palaeoclimatology, Palaeoecology*, **296**, 320–331, https://doi.org/10.1016/j.palaeo.2010.01.009

Li, S., Wignall, P.B., Xiong, Y. and Poulton, S.W. 2024. Calibration of redox thresholds in black shale: insight from a stratified Mississippian basin with warm saline bottom waters. *GSA Bulletin*, 136, 1266–1286, https://doi.org/10.1130/B36915.1

Loydell, D.K. and Cave, R. 1993. The Telychian (Upper Llandovery) stratigraphy of Buttington Brick Pit, Wales. *Newsletters on Stratigraphy*, **29**, 91–103, https://doi.org/10.1127/nos/29/1993/91

Loydell, D.K. and Cave, R. 1996. The Llandovery–Wenlock boundary and related stratigraphy in eastern mid-Wales with special reference to the Banwy River section. *Newsletters on Stratigraphy*, **34**, 39–64, https://doi.org/10.1127/nos/34/1996/39

Loydell, D.K. and Frýda, J. 2007. Carbon isotope stratigraphy of the upper Telychian and lower Sheinwoodian (Llandovery–Wenlock, Silurian) of the Banwy River section, Wales. *Geological Magazine*, **144**, 1015–1019, https://doi.org/10.1017/s0016756807003895

Loydell, D.K. and Large, R.R. 2019. Biotic, geochemical and environmental changes through the early Sheinwoodian (Wenlock, Silurian) carbon isotope excursion (ESCIE), Buttington Quarry, Wales. *Palaeogeography, Palaeoclimatology, Palaeoecology*, **514**, 305–325, https://doi.org/10.1016/j.palaeo.2018.10.028

Loydell, D.K., Frýda, J., Butcher, A. and Loveridge, R.F. 2014. A new high-resolution $\delta^{13}C_{carb}$ isotope curve through the lower Wenlock Series of Buttington Quarry, Wales. *GFF*, **136**, 172–174, https://doi.org/10.1080/11035897.2013.865668

März, C., Poulton, S.W., Beckmann, B., Küster, K., Wagner, T. and Kasten, S. 2008. Redox sensitivity of P cycling during marine black shale formation: dynamics of sulfidic and anoxic, non-sulfidic bottom waters. *Geochimica et Cosmochimica Acta*, **72**, 3703–3717, https://doi.org/10.1016/j.gca.2008.04.025

McLennan, S.M. 2001. Relationships between the trace element composition of sedimentary rocks and upper continental crust. *Geochemistry, Geophysics, Geosystems*, **2**, 2000GC000109, https://doi.org/10.1029/2000gc000109

Morford, J.L., Martin, W.R., François, R. and Carney, C.M. 2009. A model for uranium, rhenium, and molybdenum diagenesis in marine sediments based on results from coastal locations. *Geochimica et Cosmochimica Acta*, **73**, 2938–2960, https://doi.org/10.1016/j.gca.2009.02.029

Munnecke, A., Samtleben, C. and Bickert, T. 2003. The Ireviken Event in the lower Silurian of Gotland, Sweden – relation to similar Palaeozoic and Proterozoic events. *Palaeogeography, Palaeoclimatology, Palaeoecology*, **195**, 99–124, https://doi.org/10.1016/s0031-0182(03)00304-3

Oborny, S.C., Cramer, B.D., Brett, C.E. and Bancroft, A.M. 2020. Integrated Silurian conodont and carbonate carbon isotope stratigraphy of the east-central Appalachian Basin. *Palaeogeography, Palaeoclimatology, Palaeoecology*, **554**, https://doi.org/10.1016/j.palaeo.2020.109815

Pasquier, V., Bryant, R.N., Fike, D.A. and Halevy, I. 2021. Strong local, not global, controls on marine pyrite sulfur isotopes. *Science Advances*, **7**, https://doi.org/10.1126/sciadv.abb7403

Pasquier, V., Fike, D.A., Révillon, S. and Halevy, I. 2022. A global reassessment of the controls on iron speciation in modern sediments and sedimentary rocks: a dominant role for diagenesis. *Geochimica et Cosmochimica Acta*, **335**, 211–230, https://doi.org/10.1016/j.gca.2022.08.037

Poulton, S.W. 2021. *The Iron Speciation Paleoredox Proxy*. Elements in Geochemical Tracers in Earth System Science. Cambridge University Press, https://doi.org/10.1017/9781108847148

Poulton, S.W. and Canfield, D.E. 2005. Development of a sequential extraction procedure for iron: implications for iron partitioning in continentally derived particulates. *Chemical Geology*, **214**, 209–221, https://doi.org/10.1016/j.chemgeo.2004.09.003

Poulton, S.W. and Canfield, D.E. 2011. Ferruginous conditions: a dominant feature of the ocean through Earth's history. *Elements*, **7**, 107–112, https://doi.org/10.2113/gselements.7.2.107

Poulton, S. and Raiswell, R. 2002. The low-temperature geochemical cycle of iron: from continental fluxes to marine sediment deposition. *American Journal of Science*, **302**, 774–805, https://doi.org/10.2475/ajs.302.9.774

Raiswell, R. and Canfield, D.E. 1998. Sources of iron for pyrite formation in marine sediments. *American Journal of Science*, **298**, 219–245, https://doi.org/10.2475/ajs.298.3.219

Raiswell, R., Newton, R. and Wignall, P.B. 2001. An Indicator of Water-Column Anoxia: Resolution of Biofacies Variations in the Kimmeridge Clay (Upper Jurassic, U.K.). *Journal of Sedimentary Research*, **71**, 286–294, https://doi.org/10.1306/070300710286

Raiswell, R., Hardisty, D.S. *et al.* 2018. The iron paleoredox proxies: a guide to the pitfalls, problems and proper practice. *American Journal of Science*, **318**, 491–526, https://doi.org/10.2475/05.2018.03

Richardson, J.A., Lepland, A., Hints, O., Prave, A.R., Gilhooly, W.P., Bradley, A.S. and Fike, D.A. 2021. Effects of early marine diagenesis and site-specific depositional controls on carbonate-associated sulfate: insights from paired S and O isotopic analyses. *Chemical Geology*, **584**, 120525, https://doi.org/10.1016/j.chemgeo.2021.120525

Rose, C.V., Fischer, W.W., Finnegan, S. and Fike, D.A. 2019. Records of carbon and sulfur cycling during the Silurian Ireviken Event in Gotland, Sweden. *Geochimica et Cosmochimica Acta*, **246**, 299–316, https://doi.org/10.1016/j.gca.2018.11.030

Saltzman, M.R. 2001. Silurian $\delta^{13}C$ stratigraphy: a view from North America. *Geology*, **29**, 671–674, https://doi.org/10.1130/0091-7613(2001)029<0671:Scsavf>2.0.Co;2

Scotese, C. 2014. *Atlas of Silurian and Middle–Late Ordovician Paleogeographic Maps (Mollweide Projection). The Early Paleozoic, PALEOMAP Atlas for ArcGIS.* PALEOMAP Project, Evanston, IL, **5**, 73–80.

Sperling, E.A., Carbone, C., Strauss, J.V., Johnston, D.T., Narbonne, G.M. and Macdonald, F.A. 2016. Oxygen, facies, and secular controls on the appearance of Cryogenian and Ediacaran body and trace fossils in the Mackenzie Mountains of northwestern Canada. *GSA Bulletin*, **128**, 558–575, https://doi.org/10.1130/B31329.1

Stone, P. 2014. The Southern Uplands Terrane in Scotland – a notional controversy revisited. *Scottish Journal of Geology*, **50**, 97–123, https://doi.org/10.1144/sjg2014-001

Takahashi, S., Hori, R.S. *et al.* 2021. Progressive development of ocean anoxia in the end-Permian pelagic Panthalassa. *Global and Planetary Change*, **207**, https://doi.org/10.1016/j.gloplacha.2021.103650

Tribovillard, N., Algeo, T.J., Lyons, T. and Riboulleau, A. 2006. Trace metals as paleoredox and paleoproductivity proxies: an update. *Chemical Geology*, **232**, 12–32, https://doi.org/10.1016/j.chemgeo.2006.02.012

Tribovillard, N., Algeo, T.J., Baudin, F. and Riboulleau, A. 2012. Analysis of marine environmental conditions based on molybdenum–uranium covariation – applications to Mesozoic paleoceanography. *Chemical Geology*, **324–325**, 46–58, https://doi.org/10.1016/j.chemgeo.2011.09.009

Wei, G.-Y., Chen, T. *et al.* 2021. A chemical weathering control on the delivery of particulate iron to the continental shelf. *Geochimica et Cosmochimica Acta*, **308**, 204–216, https://doi.org/10.1016/j.gca.2021.05.058

Wignall, P.B. 1990. Observations on the evolution and classification of dysaerobic communities. *The Paleontological Society, Special Publications*, **5**, 99–111, https://doi.org/10.1017/S2475262200005451

Wignall, P.B. 1994. *Black Shales*. Oxford Monographs on Geology and Geophysics, **30**. Oxford University Press.

Yan, G., Lehnert, O. *et al.* 2022. The record of early Silurian climate changes from South China and Baltica based on integrated conodont biostratigraphy and isotope chemostratigraphy. *Palaeogeography, Palaeoclimatology, Palaeoecology*, **606**, 111245, https://doi.org/10.1016/j.palaeo.2022.111245

Young, S.A., Kleinberg, A. and Owens, J.D. 2019. Geochemical evidence for expansion of marine euxinia during an early Silurian (Llandovery–Wenlock boundary) mass extinction. *Earth and Planetary Science Letters*, **513**, 187–196, https://doi.org/10.1016/j.epsl.2019.02.023

Young, S.A., Benayoun, E., Kozik, N.P., Hints, O., Martma, T., Bergström, S.M. and Owens, J.D. 2020. Marine redox variability from Baltica during extinction events in the latest Ordovician–early Silurian. *Palaeogeography, Palaeoclimatology, Palaeoecology*, **554**, 109792, https://doi.org/10.1016/j.palaeo.2020.109792

Zheng, Y., Anderson, R.F., Van Geen, A. and Kuwabara, J. 2000. Authigenic molybdenum formation in marine sediments: a link to pore water sulfide in the Santa Barbara Basin. *Geochimica et Cosmochimica Acta*, **64**, 4165–4178, https://doi.org/10.1016/S0016-7037(00)00495-6

Zheng, Y., Anderson, R.F., van Geen, A. and Fleisher, M.Q. 2002. Preservation of particulate non-lithogenic uranium in marine sediments. *Geochimica et Cosmochimica Acta*, **66**, 3085–3092, https://doi.org/10.1016/S0016-7037(01)00632-9